

Torque and flux ripple mitigation technique using multi-level inverter for sequential model predictive controlled induction motor

Abobaker Kikki Abobaker, Norjulia Mohamad Nordin, Azizah Abdul Razak

Department of Electrical Power Engineering, Faculty of Electrical Engineering, Universiti Teknologi Malaysia, Johor Bahru, Malaysia

Article Info

Article history:

Received May 21, 2024

Revised Dec 1, 2024

Accepted Dec 9, 2024

Keywords:

Direct torque control

Field-oriented control

Induction motor

Multilevel inverter

Sequential model predictive control

ABSTRACT

The control of electric motors presents a fascinating topic in the field of electrical engineering. Three-phase induction motors are extensively employed in industrial applications, because of their durability and cost-effectiveness. Hence, induction motor control research remains a major priority in electrical drive technology. Field-oriented control (FOC) and direct torque control (DTC) are the most common control methods for industrial applications up to now. Recently developed microcontroller processing capabilities have enabled novel control technology like model predictive control (MPC). High-performance drive systems could benefit from this new control method. One of MPC approach, referred to as finite control set-model predictive control (FCS-MPC), focuses on reducing a single cost function. This is achieved by adjusting a weighting factor to prioritize either torque or flux error reduction. However, the primary drawbacks of the standard FCS-MPC lie in determining these weighting factors and the variable switching frequency, which greatly varies based on the operational conditions. A control approach that eliminated the weighing factor was proposed. The proposed sequential model predictive control (SMPC) method is applied to a 3-phase induction motor operated by a 5-level CHB inverter. Simulation results matched theoretical analysis. Results demonstrated that stator flux and torque are independently controlled without weighting factor, and low harmonic distortion levels.

This is an open access article under the [CC BY-SA](#) license.



Corresponding Author:

Norjulia Mohamad Nordin

Department of Electrical Power Engineering, Faculty of Electrical Engineering

Universiti Teknologi Malaysia

81310, UTM Johor Bahru, Johor, Malaysia

Email: norjulia@utm.my

1. INTRODUCTION

Model predictive control (MPC) has attracted significant interest in motor drive control, because its simple principles quick and accurate response. Additionally, MPC offers high flexibility for incorporating various constraints, making it an effective approach for complex control scenarios [1], [2]. To date, the finite control set model predictive control (FCS-MPC) for flux and torque in the induction motor (IM) has typically been executed with a singular cost function, employing a weighting factor to prioritize the minimization of either flux or torque error [3]-[5]. Determining the appropriate weighting factor presents a principal challenge within this control approach.

The design of the weighting factor is intended to normalize stator flux and torque quantities within the cost function [6]. However, choosing an appropriate weighting factor is a complex task, significantly

influencing harmonic current distortion and robustness against parameter variations. To address this challenge, the literature [7]-[14] and has suggested numerous methods to minimize or eliminate the weighting factors in MPC. According to [9], reducing the error in the voltage vector equates to reducing the error in the stator flux linkage vector. Consequently, employing space vector modulation can simplify control complex designs and reduce the computational load for selecting the best vector. The proposed method in [10], suggests using an algebraic selection of the weighting factor to achieve a performance level that is comparable to predictive current control. While this calculation is less complex than the one in [9], it still depends on machine's states and parameters. To address the challenge of selecting the weighting factor by decoupling the control variables and optimizing them individually using two cascade cost functions in [11]. However, this approach still encounters issues such as an undesired non-constant switching frequency and high ripples. A two-vector-based MPC approach that omits the use of a weighting factor. where this method maintains stable performance in steady-state conditions was discussed in [15], however, this method it increases the computational complexity, which generally not suitable for industrial applications, particularly in scenarios involving extended horizon predictions and multi-level converters.

Alternative approaches eliminate the need for a weighting factor. Preview study [8], propose a multi-objective optimization based on a ranking approach. This approach transforms the cost function values of stator flux linkage and torque for each voltage vector into ranking values. It then identifies vector with lowest average ranking value as the ideal choice. A suggested solution for decision-making involves substituting the weighting element with a fuzzy approach. Initially, a membership function transforms the cost function for stator flux linkage and torque into the range of (0, 1). After this transformation, we can use various decision functions to determine the optimal voltage vector [7]. Ignore the weighting factor in [7]-[9], [11], as it increases both the control complex designs and computational burden.

The cost function, similar to deadbeat control, ends the subsequent control period by removing the weighting element to reduce errors in tracking variables. Deadbeat flux and torque control normalizes stator flux linkage and torque references to a single vector. This approach was discussed in [16], [17]. Instead of reducing flux linkage and torque errors, the objective should be to reduce stator flux linkage vector errors. generalized sequential model predictive control (G-SMPC) [1] maintains performance regardless of cost function evaluation sequence. G-SMPC ranks control objectives by cost function evaluation sequence, with the first function being most essential. Unlike prioritized techniques, "even-handed" sequential predictive control as proposed in [18], dynamically change the control objectives. This method uses more processor resources and less customizable due to its error evaluation term.

Recent research has proposed the use of sequential model predictive control (SMPC) to eliminate the need for a weighting factor in model predictive control (MPC). This approach initially evaluates the torque cost function, selecting the two vectors with the smallest torque errors from all possible vectors. These two vectors are then assessed by a secondary cost function to identify the one that minimizes the flux discrepancy. This hierarchical structure is straightforward and removes the necessity for a weighting coefficient [12]. However, if the design prioritizes minimizing flux tracking errors as the primary cost function, the stable operation across the entire speed range is uncertain. In other words, the prior SMPC is not a universally applicable method and is effective only in specific conditions. Additionally, the use of a two-level voltage source inverter results in higher levels of total harmonic distortion (THD).

Preview study [14], a parallel predictive torque control (PPTC) method that eliminates the need for a weighting factor was introduced. The technique optimizes both torque and flux cost functions in a parallel configuration concurrently, thereby preventing the requirement for a weighting factor. However, this method results in an increased computational complexity.

Therefore, this paper introduces a sequential model predictive control (SMPC) with a 5-level cascaded H-bridge (5LCHBM) inverter. The proposed approach simultaneously optimizes torque and flux cost functions in a sequential configuration, thereby eliminating the requirement for a weighting factor and reduce the total harmonic distortion (THD). A critical aspect of this method is its ability to keep the torque and flux tracking errors within predefined limits. The remainder of the paper is organized as follows: The proposed control strategy with 5Level-CHBMI is discussed in section 2. The comparison of proposed method with DTC-5LCHBI methodology is presented in section 3. Simulation results are showcased in section 4. Section 5 concludes the paper.

2. PROPOSED CONTROL STRATEGY WITH 5LEVEL-CHBMI

This section describes the proposed control strategy (sequential model predictive control (SMPC)) with a 5-level cascaded H-bridge multilevel inverter (CHBM) to drive a three-phase induction motor in regulating speed, flux, torque, stator current, and total harmonic distortion.

2.1. Cascaded H-bridge multilevel inverter

A multilevel cascaded H-bridge (CHBM) inverter offers numerous benefits compared to multilevel neutral point-clamped and multilevel flying capacitors inverters. The CHBM inverter is modular and more straightforward to manage due to the uniform structure of each cell. Additionally, it enables achieving a high number of levels with a minimal quantity of required components. These components help reduce switching losses in the devices, enhancing both the reliability and efficiency of the circuit. Consequently, this topology is extensively employed in industrial applications, particularly in photovoltaic systems [19].

Figure 1 shows a three-phase 5-level cascaded H-bridge (CHBM) inverter. In this configuration, each phase comprises of several power cells serially arranged where each power cell is a single-phase H-bridge inverter. It is assumed that each phase contains 'n' number of such cells, and each cell is supplied by a separate dc source, denoted as V_{dc}. The power switches within each cell produce three different voltage levels: V_{dc}, 0, and [-V_{dc}, which correspond to the cell states {1, 0, -1} respectively [20], [21]. The overall voltage level of each phase is the aggregate of the voltage levels of all its cells given as (1).

$$S_x = \sum_{i=1}^n S_{xi} \tag{1}$$

The total possible number of voltage levels for each phase can be expressed as (2).

$$m = 2n + 1 \tag{2}$$

The voltages for each phase of the inverter are determined through (3)-(5).

$$V_{aN} = V_{dc}[(S_{a12} - S_{a22}) + (S_{a11} - S_{a21})] \tag{3}$$

$$V_{bN} = V_{dc}[(S_{b12} - S_{b22}) + (S_{b11} - S_{b21})] \tag{4}$$

$$V_{cN} = V_{dc}[(S_{c12} - S_{c22}) + (S_{c11} - S_{c21})] \tag{5}$$

The voltage in the d-q frame is expressed as (6) and (7).

$$V_{sd} = \frac{1}{3}(2V_{aN} - V_{bN} - V_{cN}) \tag{6}$$

$$V_{sq} = \frac{1}{\sqrt{3}}(V_{bN} - V_{cN}) \tag{7}$$

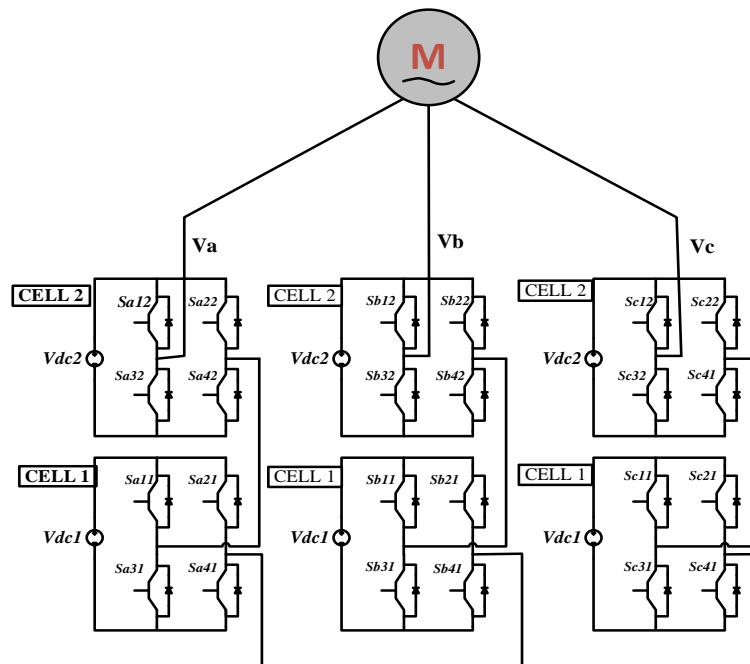


Figure 1. Three-phase 5-level CHB inverter

In a multilevel cascaded H-bridge inverter, multiple combinations of switching states can produce identical voltage vectors. Therefore, the count of unique, nonredundant voltage vectors, can be calculated using (8), where n is the cell number per phase. The three-phase 5LCHBMI utilized in this research, 125 potential switching states within the static d-q coordinate system. These switching states correspond to 61 different voltage vectors [22].

$$K_v = 12n^2 + 6n + 1 \quad (8)$$

2.2. Mathematical model of induction motor

The stator flux is generated through coupling of stator current and rotor current while the coupling of rotor current and stator current generates the rotor flux of a three-phase induction motor. The flux equation is as (9) and (10).

$$\psi_s = L_s i_s + L_m i_r \quad (9)$$

$$\psi_r = L_m i_s + L_r i_r \quad (10)$$

Where ψ_s is the stator flux and ψ_r denote the rotor flux. Similarly, i_s and i_r represent the stator current and rotor current, respectively. The terms L_s , L_r , and L_m refer to the stator, rotor, and mutual inductances, respectively.

The system model as articulated in a stationary frame delineate as (11)-(14) where ω is the rotor's angular velocity.

$$v_s = R_s \cdot i_s + \frac{d\psi_s}{dt} \quad (11)$$

$$0 = R_r \cdot i_r + \frac{d\psi_r}{dt} - j \cdot \omega \cdot \psi_r \quad (12)$$

$$T = \frac{3}{2} p |\Psi_s \otimes i_s| \quad (13)$$

$$J \frac{d\omega}{dt} = T - T_L \quad (14)$$

In this context, v_s is the stator voltage vector, while R_s and R_r indicate the equivalent stator and rotor resistances, respectively. \otimes represents cross product of two complex vectors. The load torque and electromagnetic torque are represented by T_L and T respectively, while ω is the electrical speed.

2.3. Prediction equations

For the evaluation of torque and flux cost functions, accurate prediction of torque and flux cost functions is essential for all possible switching states. The torque and stator flux predictions are derived using discrete-time equations off the rotor flux calculation can be derived from the equivalent (10) and (12) which described the rotor dynamics of an IM within a rotating reference frame, aligned with the rotor winding. This derivation yields the value of Ψ_r .

$$\Psi_r + \tau_r \frac{d\Psi_r}{dt} = L_m i_s \quad (15)$$

Where, $\tau_r = L_r/R_r$ denotes the rotor time constant. By applying the forward-Euler discretization technique and taking T_s as the sampling time, the discrete-time equation for estimating the rotor flux is articulated is given by (16).

$$\Psi_r^k = \left(1 - \frac{T_s}{\tau_r}\right) \Psi_r^{k-1} + L_m \frac{T_s}{\tau_r} i_s^{k-1} \quad (16)$$

By using (9) and (10), the stator flux estimation is achieved using (17).

$$\Psi_s^k = \frac{L_m}{L_r} \Psi_r^k + \left(1 - \frac{L_m^2}{L_s L_r}\right) i_s^k \quad (17)$$

Using (11), the stator flux prediction is found by utilizing the forward-Euler discretization method as (18).

$$\Psi_s^{k+1} = \Psi_s^k + T_s v_s^k - T_s R_s i_s^k \tag{18}$$

Furthermore, the prediction of stator current is derived through the application of the forward-Euler discretization method, as indicated by (19).

$$i_s^{k+1} = C_1 i_s^k + C_2 \Psi_s^k + \frac{T_s}{L_\sigma} v_s^k \tag{19}$$

Where, $R_\sigma = (R_s + (L_r L_m)^2 R_r)$ is the equivalent resistance as referred to the stator, with $C_1 = (1 - (R_\sigma T_s / L_\sigma))$, and $C_2 = (L_m / L_r) T_s / L_\sigma ((1 / \tau_r) - j \omega_k)$, in this formulation, L_σ is the leakage inductance, τ_r is the rotor time constant, and σ is the total leakage factor as shown in (20) and (21) respectively.

$$L_\sigma = \sigma L_s \tag{20}$$

$$\tau_r = \frac{L_r}{R_r} \tag{21}$$

The prediction of torque is based on prediction of stator flux and stator current, which defined as in (22).

$$T^{k+1} = \frac{3}{2} p |\Psi_s^{k+1} \otimes i_s^{k+1}| \tag{22}$$

2.4. Proposed control strategy

Figure 2 shows a block diagram of the proposed induction machine drives system, SMPC with 5-level CHBM inverter forming a cascade structure for managing multiple control objectives. The scheme utilizes a series of cost functions, each tailored to a specific control objective. Rather than applying a single cost function encompassing various objectives connected through a weighting factor, the approach addresses the problem by employing separate cost functions, with each one focused on a separate control objective.

It is important to acknowledge that when implementing the predictive control strategy, there is need to consider the delay in applying the optimal vector. This is due to the fact that the processes of measurements, data processing, and optimization algorithms are not instantaneous. To offset this delay, the control variables ought to be forecasted for the future instant (k + 2). To address this delay, consider the computation time and implement the chosen switching state after the following sampling instant. The control algorithm is adjusted in this manner. The process involves measuring i_s and ω , applying the switching state, estimating Ψ_s^k and Ψ_r^k values at time t_{k+1} , predicting Ψ_s^k and Ψ_r^k values for the next sampling instant t_{k+2} , evaluating the cost function, and selecting the minimizing switching state [23].

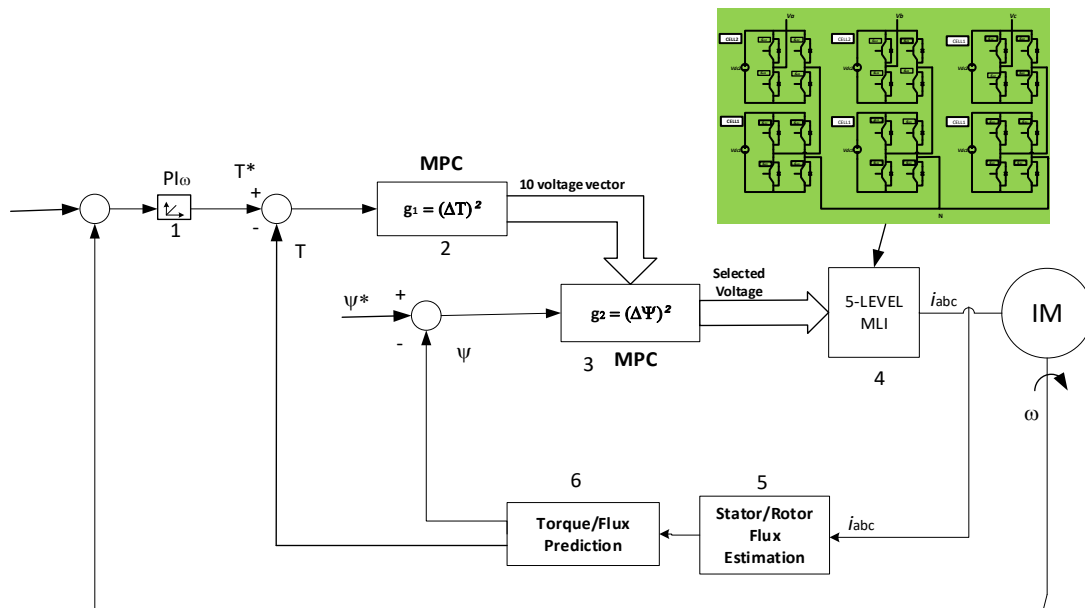


Figure 2. Proposed control model

In Figure 2, the difference between the reference speed (ω^*) and the actual measured speed (ω) is fed into a proportional-integral (PI) controller in block 1 in Figure 2. The controller then produces the reference torque (T^*). The cost function utilized for torque control (g_1) is obtained as (23).

$$g_1 = (T^* - T^{k+2})^2 \quad (23)$$

Where T^{k+2} represents the predicted torque, determined as (24).

$$T^{k+2} = \frac{3}{2} p |\Psi_s^{k+2} \otimes i_s^{k+2}| \quad (24)$$

Consequently, in block 2 of the block diagram in Figure 2, g_1 is computed for each of the 61 different voltage vectors produced by the inverter. However, ten voltage vectors yielding the lowest values of g_1 (i.e., the most minor error) are chosen for the subsequent control steps. This step aligns with the minimization of flux error, executed through the cost function g_2 , which is associated with the flux error and is defined by (25).

$$g_2 = (\Psi_s^* - |\Psi_s^{k+2}|)^2 \quad (25)$$

Where Ψ_s^{k+2} represents the predicted flux, which is calculated as (26).

$$\Psi_s^{k+2} = \Psi_s^{k+1} + T_s v_s^{k+1} - T_s R_s i_s^{k+1} \quad (26)$$

The cost function is methodically assessed for each of the ten voltage vectors chosen in the preceding torque control step. Ultimately, the voltage vector that optimally minimizes g_2 is determined and subsequently supplied to the load. This process is depicted in block 3 of Figure 2. Block 4 in Figure 2 shows the power circuit of the 5-level CHBM inverter, block 5 corresponds to (16) and (17) for estimating flux, and block 6 gives (17) and (26) for predicting torque and flux.

The flowchart of the proposed control strategy is illustrated in Figure 3 (see Appendix). The strategy commences by monitoring the stator current (i_s) and the speed at a specified sampling interval denoted as (k), as illustrated in step 1. The voltage vector computed during the preceding sampling interval is subsequently applied in step 2. Step 3 involves the estimation of both the stator flux and rotor flux at the specified sampling interval k . Subsequently, in step 4, the parameter g_1 is computed for all 61 voltage vectors. Step 5 involves the selection of ten voltage vectors characterized by the smallest values of g_1 . In step 6, the parameter g_1 is computed for the ten previously selected voltage vectors. Ultimately, in step 7, the voltage vector that minimizes the parameter g_1 is chosen to be applied in the subsequent sampling interval [24].

3. COMPARISON WITH DTC-5LCHBI METHODOLOGY

To determine the positive attributes of the proposed control strategy, the performance of the proposed control model is compared with that of DTC-5LCHBMI. A significant difference exists between the SMPC-5LCHBMI and DTC-5LCHBMI as seen from the two block diagrams Figures 2 and 4. In DTC-5LCHB, eight levels of hysteresis are used for torque and five hysteresis used for the flux.

3.1. DTC-5LCHBMI

In traditional direct torque control (DTC), selecting the right voltage vector from a 2-level inverter regulates flux and torque. This sort of inverter applies the same voltage vector regardless of torque and flux error due to its limited voltage vector set. The control structure uses hysteresis controllers, a look-up table, a 5-level cascaded H-bridge multilevel inverter (CHBMI), flux and torque estimators. These estimators estimate torque, flux, and sector using voltage and current data. Eight-level and five-level hysteresis controllers represent torque and flux controllers. The torque, flux, and sector statuses in the look-up table determine the inverter voltage vector [22].

A 5-level cascaded H-bridge multilevel inverter (CHBMI) provides more torque and flux regulation voltage vector possibilities. Increased flexibility improves direct torque control's dynamic performance. Figure 4 shows the system block diagram. A 5-level CHBMI has many voltage vector selection options, therefore, a control system is needed to choose the optimal voltage vectors for DTC drive dynamic performance. To determine the optimal vector, the flux and torque hysteresis comparators must have more levels than the standard 2-level inverter-based DTC [25].

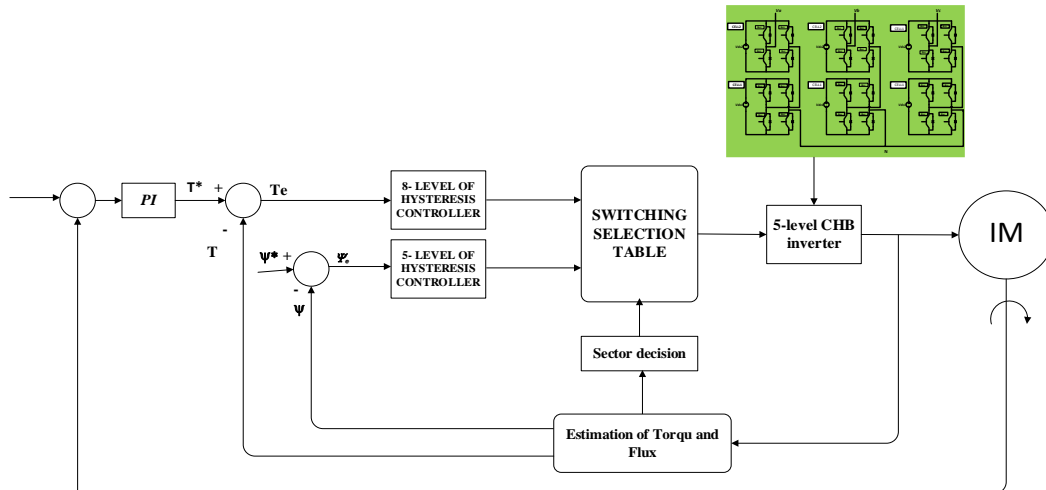


Figure 4. Block diagram of DTC-5LCHBI

4. RESULTS AND DISCUSSION

This section presents the simulation results of the control performance of the proposed sequential model predictive control (SMPC). The simulation is performed with MATLAB/Simulink simulation software. The target system for the implemented control scheme is an induction motor derived by 5-level CHB inverter. The proposed model results are compared with the conventional DTC-5LCHBI results. Details of the parameters used for the simulation are presented in Table 1.

Table 1. System parameters

Parameter	Value	Parameter	Value
Stator resistance, R_s	3 Ω	Number of poles, P	4
Rotor resistance, R_r	3.793 Ω	Combined inertia, J	0.02799 kg-m ²
Stator self-inductance, L_s	0.3308 H	Combined viscous friction, B	0.01025 N.m.s
Rotor self-inductance, L_r	0.3308 H	DC link voltage (per phase), VDC	165 V
Mutual inductance, L_m	0.3049 H	Stator flux reference,	0.896 Wb
Reference speed ω^*	149.6 rad/s	Load torque	10 Nm

To validate the performance of the proposed control scheme, various parameters variations with time are tested as shown in Figures 5-8. In Figure 5 shows that comparative results of the rotor speed of both control algorithms. Figure 5(a) shows dynamic drive speed response from rest to 149.6 rad/sec and compares it to ω -ref. At 0.28 seconds, the rotor speed matches the reference speed and remains the same. Results indicate that the control mechanism performs. Figure 5(b). this is rotor speed variation. Both control algorithms achieve and maintain the reference speed with minimal variation. The research findings demonstrate their speed monitoring effectiveness. Both control methods regulate speed similarly in the system settings and parameters evaluated.

Figure 6 shows the variation magnetic flux. Figure 6(a) shows the variation magnetic flux (flux-SMPC) and the reference flux (flux-ref) with time for the proposed control strategy. It can be seen that the magnetic flux of the IM and follows the reference flux at 0.87 Wb immediately from the starting point ($t = 0$).

Figure 6(b) shows the variation in flux linkage for both control methods. It appears that there are visible ripples in the flux linkage for both control methods. However, the ripples are dominant in the DTC method compared to SMPC method. The DTC method exhibits larger flux oscillations during steady-state operation, indicating a higher level of ripple compared to the SMPC method, which shows more stable behavior. The SMPC control appears to track the reference flux more closely with fewer fluctuations, suggesting superior performance in maintaining flux stability. However, both strategies generally maintain the flux at the desired level after the initial rise, ensuring effective control after transient conditions. In steady-state operation, the DTC method has more flux oscillations and ripple than the SMPC method, which is more stable. The SMPC control tracks the reference flux more precisely and with fewer deviations, ensuring flux stability. Both systems usually maintain the flow at the intended level after the initial increase, ensuring efficient management during changes in conditions.

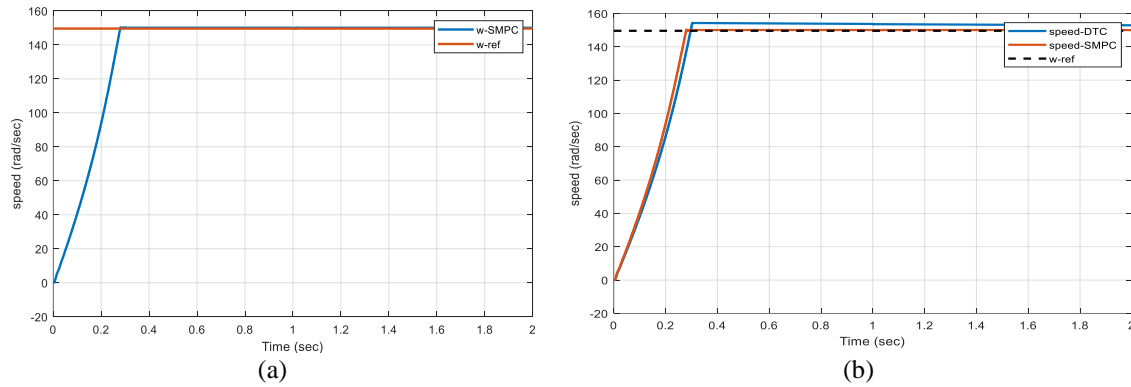


Figure 5. Reference speed and rotor speed: (a) reference speed and rotor speed of SMPC and (b) comparison results between SMPC and DTC

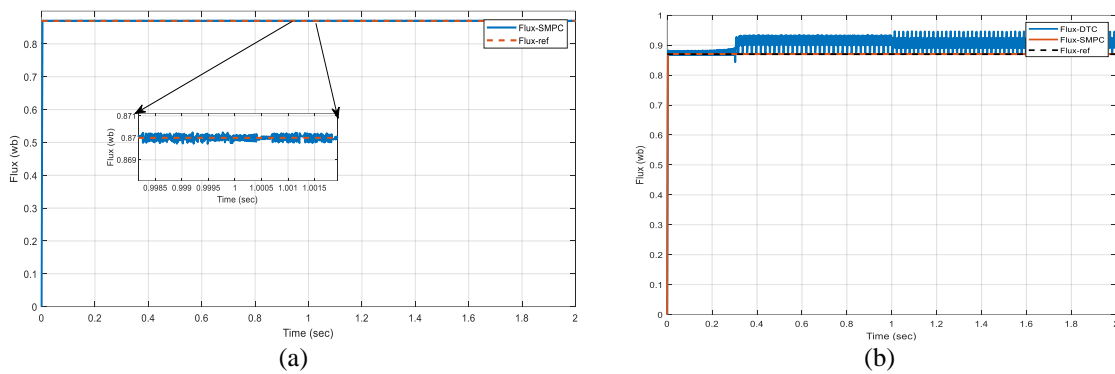


Figure 6. Reference flux and flux: (a) reference stator flux and stator flux of SMPC and (b) comparison results between SMPC and DTC

Furthermore, Figure 7 the electromagnetic torque response, Figure 7(a) illustrates the electromagnetic torque variation with time. As seen the electromagnetic torque shows a dynamic response at the initial stage, with rapid change in levels that include positive and negative values, in a transient response between 0 sec to 0.28 sec, after which the torque remains stable. At 1 sec when the load torque is 10 Nm, there is a notable spike in the torque for a short duration, after which the torque returns to relatively steady state with minor ripples.

The electromagnetic torque variation for the two control methods is shown Figure 7(b) with both strategies show a rapid increase in torque between 0 sec and 0.3 sec. After the initial transient period at (0.3 sec to 1 sec), the torque in the DTC shows significant ripples, while the torque in the SMPC is smoother and has a smaller steady-state ripple. In the transit state (load = 10 Nm, t = 1 sec), the torque increase for both control strategies with higher torque ripple in SMPC than in DTC method.

The simulation waveform for the variation of stator current with time is depicted in Figure 8(a). At starting, there is a noticeable spike of magnitude 20 A, which rapidly decreases in amplitude of 2.8 A from 0.3 sec to 1 sec. after which the current increased during a load step to around 6 A. In Figure 8(b), depicts the comparative waveform of parameters for the proposed SMPC-5LCHB and DTC-5LCHB. The stator current variation with time for the two-control methods DTC and SMPC is illustrated in Figure 8(b). At observed, between 0 sec to 0.3 sec the DTC and SMPC current show a large transient response with high peaks, after this the SMPC current appears to stabilize more rapidly into a steady state with fewer ripples compared to the DTC current. SMPC has a more constant current response and lower ripple during steady state, suggesting better current control than DTC.

The total harmonic distortion for the DTC-5LCHB is shown in Figure 9. As noted, the DTC-5LCHB has a THD of 9.86%, which is more when compared to the THD of the proposed strategy 5.68%. In summary, SMPC improves speed, flux control, harmonic distortion reduction, and smoother stator current behavior. However, DTC excels at providing a more constant torque response with fewer fluctuations. SMPC performs better with less oscillation and better efficiency.

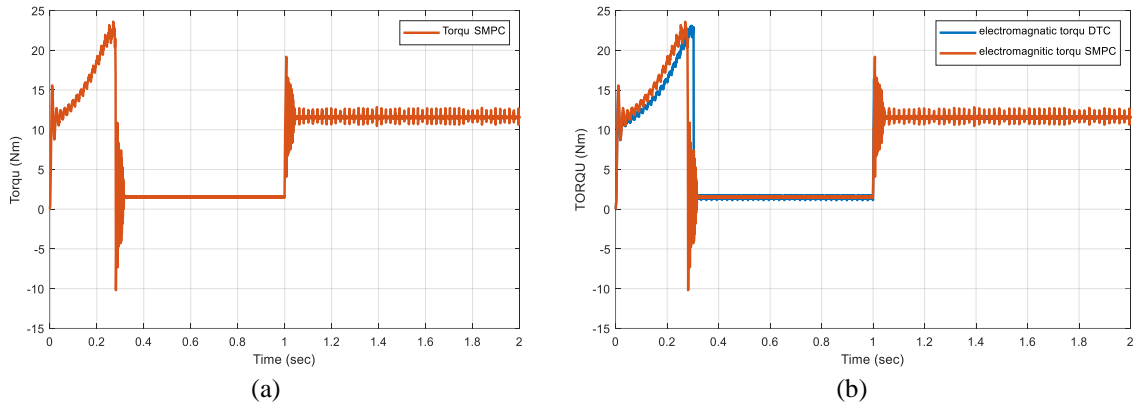


Figure 7. Electromagnetic torque response: (a) torque of SMPC and (b) comparison results between SMPC and DTC

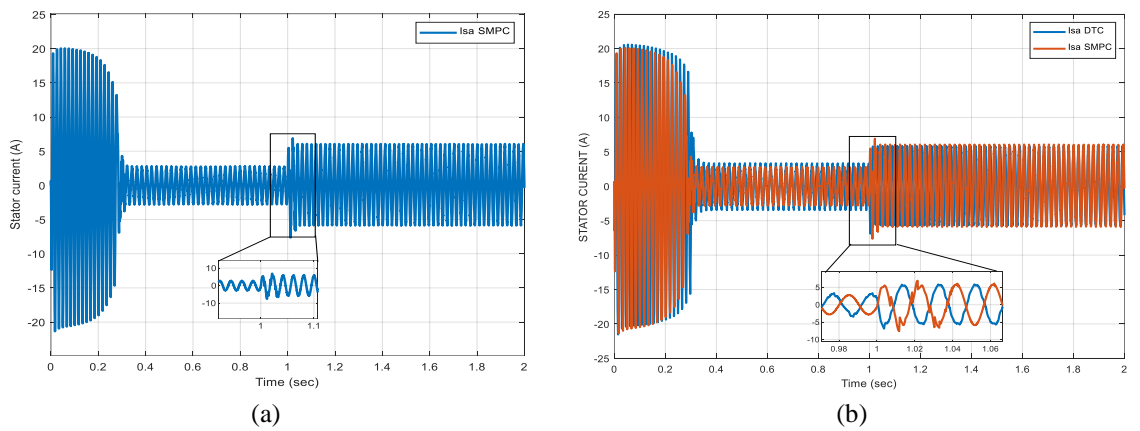


Figure 8. Stator current: (a) stator current of SMPC and (b) comparison results between SMPC and DTC

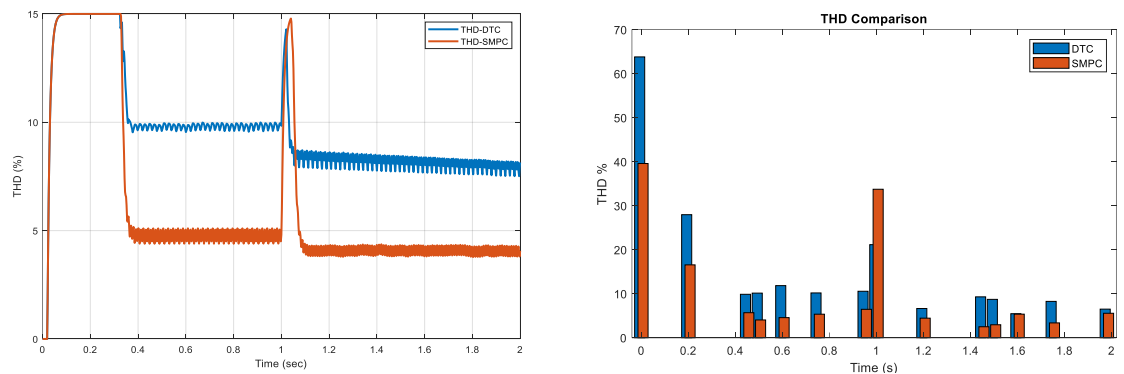


Figure 9. Stator current THD: Comparative results between SMPC-5LCHB and DTC-5LCHB

5. CONCLUSION

This paper introduces a novel approach for high-performance control of an induction motor. The approach uses a model predictive control, utilizing the fundamental equations of the machine and the inverter. Simulation outcomes validate that this strategy effectively reduces controls torque, flux and the THD current around 5.68% compared with DTC around 9.86%. Furthermore, the use of weighting factors has been eliminated in the regulation of flux and torque in predictive control. A novel SMPC algorithm has been developed for 5L-CHBMI 3phase inverter. The proposed technique takes into account a subset of all potential voltage vectors, with the aim of minimizing the number of computations required and ensuring its compatibility with standard control platform. Ultimately, the SMPC-5LCHBMI's findings affirm the potential of this strategy as an appealing and promising option for high-performance AC drives.

APPENDIX

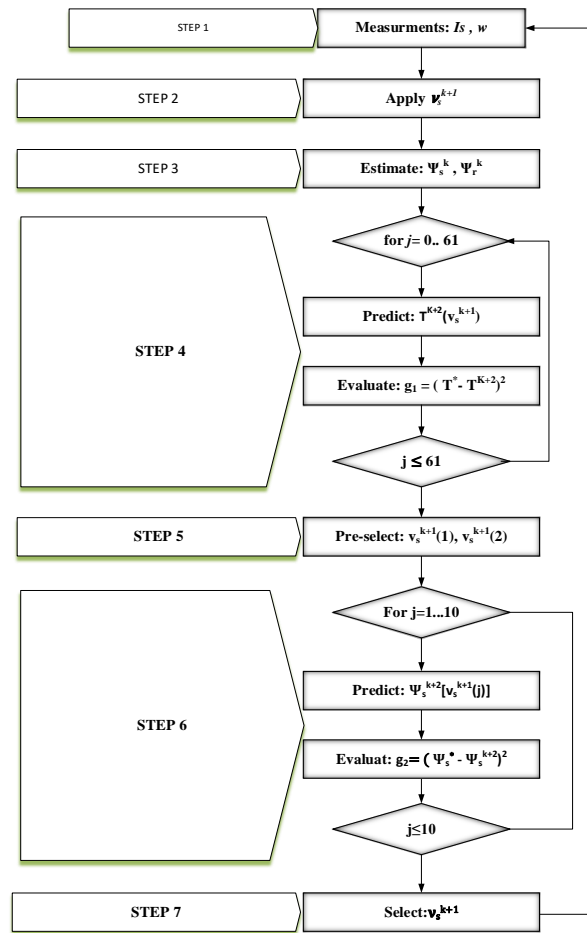


Figure 3. Flowchart of proposed control scheme




REFERENCES

- [1] Y. Zhang, B. Zhang, H. Yang, M. Norambuena, and J. Rodriguez, "Generalized sequential model predictive control of IM drives with field-weakening ability," *IEEE Transactions on Power Electronics*, vol. 34, no. 9, pp. 8944–8955, Sep. 2019, doi: 10.1109/TPEL.2018.2886206.
- [2] F. Wang, Z. Zhang, X. Mei, J. Rodriguez, and R. Kennel, "Advanced control strategies of induction machine: Field oriented control, direct torque control and model predictive control," *Energies*, vol. 11, no. 1, p. 120, Jan. 2018, doi: 10.3390/en11010120.
- [3] J. Holtz, "Advanced PWM and predictive control—an overview," *IEEE Transactions on Industrial Electronics*, vol. 63, no. 6, pp. 3837–3844, Jun. 2016, doi: 10.1109/TIE.2015.2504347.
- [4] P. Karamanakos and T. Geyer, "Model predictive torque and flux control minimizing current distortions," *IEEE Transactions on Power Electronics*, vol. 34, no. 3, pp. 2007–2012, Mar. 2019, doi: 10.1109/TPEL.2018.2862253.
- [5] H. T., A. V. R. Teja, G. Bhuvaneswari, and B. Singh, "Performance enhancement in a multilevel inverter fed PTC induction motor drive by optimal voltage vector selection," *International Journal of Power Electronics and Drive Systems (IJPEDS)*, vol. 10, no. 2, pp. 801–812, Jun. 2019, doi: 10.11591/ijped.v10.i2.pp801-812.
- [6] M. Mamdouh, M. A. Abido, and Z. Hamouz, "Weighting factor selection techniques for predictive torque control of induction motor drives: A comparison study," *Arabian Journal for Science and Engineering*, vol. 43, pp. 433–445, Feb. 2018, doi: 10.1007/s13369-017-2842-2.
- [7] C. A. Rojas, J. R. Rodriguez, S. Kouro, and F. Villarroel, "Multiobjective fuzzy-decision-making predictive torque control for an induction motor drive," *IEEE Transactions on Power Electronics*, vol. 32, no. 8, pp. 6245–6260, Aug. 2017, doi: 10.1109/TPEL.2016.2619378.
- [8] C. A. Rojas, J. Rodriguez, F. Villarroel, J. R. Espinoza, C. A. Silva, and M. Trincado, "Predictive torque and flux control without weighting factors," *IEEE Transactions on Industrial Electronics*, vol. 60, no. 2, pp. 681–690, Feb. 2013, doi: 10.1109/TIE.2012.2206344.
- [9] Y. Zhang, Y. Bai, and H. Yang, "A universal multiple-vector-based model predictive control of induction motor drives," *IEEE Transactions on Power Electronics*, vol. 33, no. 8, pp. 6957–6969, Aug. 2018, doi: 10.1109/TPEL.2017.2754324.
- [10] T. Geyer, "Algebraic weighting factor selection for predictive torque and flux control," in *2017 IEEE Energy Conversion Congress and Exposition (ECCE)*, IEEE, Oct. 2017, pp. 357–364. doi: 10.1109/ECCE.2017.8095804.
- [11] V. Vodola *et al.*, "Sequential MPC strategy for high performance induction motor drives: a detailed analysis," in *2019 IEEE Energy Conversion Congress and Exposition (ECCE)*, IEEE, Sep. 2019, pp. 6595–6600. doi: 10.1109/ECCE.2019.8912708.
- [12] M. Norambuena, J. Rodriguez, Z. Zhang, F. Wang, C. Garcia, and R. Kennel, "A very simple strategy for high-quality performance of ac machines using model predictive control," *IEEE Transactions on Power Electronics*, vol. 34, no. 1, pp. 794–800, Jan. 2019, doi: 10.1109/TPEL.2018.2812833.




- [13] Z. Wang, H. Guo, Z. Ping, Y. Wang, and Z. Zhang, "Revised sequential predictive torque control with adaptability under multiple operating conditions for induction motors drives," in *2021 IEEE International Conference on Predictive Control of Electrical Drives and Power Electronics (PRECEDE)*, IEEE, Nov. 2021, pp. 502–506, doi: 10.1109/PRECEDE51386.2021.9681043.
- [14] F. Wang, H. Xie, Q. Chen, S. A. Davari, J. Rodriguez, and R. Kennel, "Parallel predictive torque control for induction machines without weighting factors," *IEEE Transactions on Power Electronics*, vol. 35, no. 2, pp. 1779–1788, Feb. 2020, doi: 10.1109/TPEL.2019.2922312.
- [15] Y. Zhang, Y. Peng, and H. Yang, "Performance improvement of two-vectors-based model predictive control of PWM rectifier," *IEEE Transactions on Power Electronics*, vol. 31, no. 8, pp. 6016–6030, Aug. 2016, doi: 10.1109/TPEL.2015.2498306.
- [16] Y. Zhang, H. Yang, and B. Xia, "Model-predictive control of induction motor drives: torque control versus flux control," *IEEE Transactions on Industry Applications*, vol. 52, no. 5, pp. 4050–4060, Sep. 2016, doi: 10.1109/TIA.2016.2582796.
- [17] Y. Zhang and H. Yang, "Two-vector-based model predictive torque control without weighting factors for induction motor drives," *IEEE Transactions on Power Electronics*, vol. 31, no. 2, pp. 1381–1390, Feb. 2016, doi: 10.1109/TPEL.2015.2416207.
- [18] S. A. Davari, M. Norambuena, V. Nekoukar, C. Garcia, and J. Rodriguez, "Even-handed sequential predictive torque and flux control," *IEEE Transactions on Industrial Electronics*, vol. 67, no. 9, pp. 7334–7342, Sep. 2020, doi: 10.1109/TIE.2019.2945274.
- [19] Y. Babkrani, A. Naddami, and M. Hilal, "A smart cascaded H-bridge multilevel inverter with an optimized modulation techniques increasing the quality and reducing harmonics," *International Journal of Power Electronics and Drive Systems (IJPEDS)*, vol. 10, no. 4, pp. 1852–1862, Dec. 2019, doi: 10.11591/ijpeds.v10.i4.pp1852-1862.
- [20] P. S. Gnanamurthy and V. Govindasamy, "Analysis of cascaded H-bridge multilevel inverter with current control methods," *International Journal of Power Electronics and Drive Systems (IJPEDS)*, vol. 13, no. 2, pp. 998–1006, Jun. 2022, doi: 10.11591/ijpeds.v13.i2.pp998-1006.
- [21] M. A. I. Aljewari, A. Jidin, S. A. A. Tarusan, and M. Rasheed, "Implementation of SVM for five-level cascaded H-bridge multilevel inverters utilizing FPGA," *International Journal of Power Electronics and Drive Systems (IJPEDS)*, vol. 11, pp. 1132–1144, Sep. 2020, doi: 10.11591/ijpeds.v11.i3.pp1132-1144.
- [22] S. A. A. Tarusan, A. Jidin, and M. L. M. Jamil, "The simulation analysis of torque ripple reduction by using optimal voltage vector in DTC fed by five-level CHB inverter," *Indonesian Journal of Electrical Engineering and Computer Science*, vol. 20, no. 3, pp. 1665–1676, Dec. 2020, doi: 10.11591/ijeecs.v20.i3.pp1665-1676.
- [23] P. Cortes, J. Rodriguez, C. Silva, and A. Flores, "Delay compensation in model predictive current control of a three-phase inverter," *IEEE Transactions on Industrial Electronics*, vol. 59, no. 2, pp. 1323–1325, Feb. 2012, doi: 10.1109/TIE.2011.2157284.
- [24] A. K. Abobaker, N. M. Nordin, N. A. Azli, R. Ayop, and N. A. M. Subha, "Model predictive control for induction motor fed by 5-level cascaded H-bridge inverter," in *Mahyuddin, N.M., Mat Noor, N.R., Mat Sakim, H.A. (eds) Proceedings of the 11th International Conference on Robotics, Vision, Signal Processing and Power Applications*, Singapore: Springer, 2022, pp. 144–149, doi: 10.1007/978-981-16-8129-5_23.
- [25] N. M. Nordin, N. R. N. Idris, and N. A. Azli, "Direct torque control with 5-level cascaded H-bridge multilevel inverter for induction machines," in *IECON 2011 - 37th Annual Conference of the IEEE Industrial Electronics Society*, IEEE, Nov. 2011, pp. 4691–4697, doi: 10.1109/IECON.2011.6120084.

BIOGRAPHIES OF AUTHORS






Abobaker Kikki Abobaker    received the B.Sc. degree in electrical engineering from The College of Technical Sciences, Sabha, Libya, in 2002, and an M.S. degree in electrical engineering from Sam Higginbottom University of Agriculture, Technology and Sciences (SHUATS), Allahabad, India, in 2017. He is currently pursuing a Ph.D. degree with Universiti Teknologi Malaysia (UTM). He has taught courses in control engineering, and electrical systems. He is also a full-time faculty member at The Higher Institute of Technical Sciences, Ghat. His research interests include model predictive control of power converters and drives. He can be contacted at email: kikki@graduate.utm.my.



Norjulia Mohamad Nordin    received her degree in Bachelor of Engineering in Electrical Engineering from the Universiti Teknologi Malaysia (UTM) in 2006 and the Master in Engineering Science (energy system) from the University of New South Wales in 2008. She then received her Ph.D. in Electrical Engineering from UTM in 2016. Currently, she is a Senior Lecturer at the Faculty of Electrical Engineering, Universiti Teknologi Malaysia (UTM). Her current research interests are in AC motor drives/electrical drives, bidirectional converters, wide bandgap device for power electronics converters, power electronic applications, electrical machines, and renewable energy conversion. She can be contacted at email: norjulia@utm.my.



Azizah Abdul Razak    received the B.Sc. degree in electrical engineering (computer) from UTHM (Universiti Tun Hussein Onn Malaysia), in 2006, and an M.Sc. degree in electrical power from UTM (Universiti Teknologi Malaysia), in 2018. She is currently pursuing a Ph.D. degree with the Department of Electrical Engineering at Universiti Teknologi Malaysia (UTM), current research interests include power electronics and control systems. She can be contacted at email: azizah48@graduate.utm.my.